

Fast quantum Monte Carlo on a GPU

Y. Lutsyshyn*

Institut für Physik, Universität Rostock, 18051 Rostock, Germany

Abstract

We present a scheme for the parallelization of quantum Monte Carlo on graphical processing units, focusing on bosonic systems and variational Monte Carlo. We use asynchronous execution schemes with shared memory persistence, and obtain an excellent acceleration. Comparing with single core execution, GPU-accelerated code runs over $\times 100$ faster. The CUDA code is provided along with the package that is necessary to execute variational Monte Carlo for a system representing liquid helium-4. The program was benchmarked on several models of Nvidia GPU, including Fermi GTX560 and M2090, and the latest Kepler architecture K20 GPU. Kepler-specific optimization is discussed.

Keywords:

Quantum Monte Carlo, GPU, CUDA, Quantum liquid, Liquid ^4He

1. Introduction

Quantum Monte Carlo (QMC) is an umbrella term for a family of first-principles methods for solving quantum many-body problems. QMC are the methods of choice for describing correlated quantum liquids and solids, with a wide range of applications. The methods scale well and can be used on systems with hundreds and even thousands of particles. They are nonetheless computationally expensive, creating a demand for efficient parallelization schemes. In this work we present a parallelization of QMC for graphical processing units (GPU).

*Corresponding author.

Email address: `email address` (Y. Lutsyshyn)

URL: `www.physik.uni-rostock.de/qtmps` (Y. Lutsyshyn)

A GPU processor is built with a number of transistors which is comparable to that of a modern CPU, but allocates more transistors to the arithmetic logical units, commonly called single processor cores. A GPU from the Nvidia Kepler family, for example, hosts over two thousand such “cores”. When properly programmed, GPUs allow to execute numerical algorithms with significant acceleration. However, the large number of GPU cores are created in exence of the cache memory and control units. The challenge is to supply such a large number of cores with enough workload and to avoid serialization.

Several groups had published successful GPU parallelization for quantum Monte Carlo schemes. Most of these works relate to QMC methods that either operate in the second quantization picture or use an expansion in finite basis sets and thus find their bottlenecks in operations on very large matrices, or even in the generation of pseudorandom number sequences [1–3]. The method that is considered here uses the real-space representation of states, and the numerical challenges lie in the calculation of pair distances, estimation of wavefunctions and expectation values. Numerically, QMC in space representation is rather different from the above methods.

While the real-space representation for QMC is a wide-spread approach, GPU parallelization of such methods has only been reported in Refs. [4, 5]. Anderson, Goddard, and Schröder descibed their GPU efforts in 2007 [4]. This early implementation masked the data structures as graphical objects and used a GPU to process them. Such an approach necessarily had significant limitations. Nevertheless, Anderson et al. achieved acceleration, comparing to a single-core execution, up to a factor of $\times 7$. The Amdahl law [6] was indicated as a significant limitation in [4]. Presently, GPU may be programmed with specially designed languages, most notably with CUDA for Nvidia GPUs. Recently, Elser, Kim, Ceperley, and Shulenburger reported a CUDA implemmentation for the QMCPack package [5]. Compared to the execution on four cores of a Xeon processor, the GPU-parallelized code ran up to $\times 16$ times faster. These two works established certain approaches, in particular, a succesful use of the mixed precision for representing floating point numbers. It should be noted that while works [4, 5] considered both variational and diffusion Monte Carlo, this work is limited to variational Monte Carlo (VMC). Also, both of Refs. [4, 5] dealt with fermionic wavefuncions for electrons, as is necessary for representing material properties. Fermionic wavefunctions are mathematically more involved than the bosonic ones, in the sense that they contain more arithmetics per memory fetch. The present

work deals with a bosonic quantum liquid, in particular with liquid helium, and uses a very simple wavefunction. Having fewer mathematical operations with respect to loop iterations, memory transactions, and conditional expressions, such a calculation is, arguably, more difficult to parallelize effectively. However, levels of acceleration were achieved that exceed those reported in Ref. [5]. This only became possible through several enhancements. In particular, asynchronous walker writeouts from GPU to host memory has allowed to limit reloading of walkers into the shared memory of the GPU. As the essential data remains loaded into high-level memory of the GPU for multiple steps, the GPU proceeds generating new configurations without delay. For the new Kepler family of Nvidia GPUs, we made use of its very large register space, allowing for better occupancy of the GPU. Asynchronous kernel execution allowed masking of the CPU load by the GPU run times, thus circumventing the Amdahl limit. These and several other features are described in detail below, and a working minimal code is provided.

2. Variational Monte Carlo

Variational Monte Carlo relies on the variational principle which provides that for any approximate wavefunction ψ of some system with Hamiltonian \hat{H} , its ground-state energy E_0 is limited from above by

$$E_0 \leq \frac{\langle \psi | \hat{H} | \psi \rangle}{\langle \psi | \psi \rangle}. \quad (1)$$

Minimization of the r.h.s. of Eq. (1) with respect to ψ yields an upper bound for the ground state energy E_0 . Optimized trial wavefunction ψ may be taken as the best guess for the true ground state of the system. Physical properties are extracted by evaluating the expectation values of their corresponding quantum operators,

$$\langle A \rangle = \frac{\langle \psi | \hat{A} | \psi \rangle}{\langle \psi | \psi \rangle}. \quad (2)$$

In particular, optimization of the trial wavefunction is the minimization of $\langle \hat{H} \rangle$. The optimized variational wavefunction is also used for importance sampling in first-principles many-body calculations, in particular the diffusion Monte Carlo and sometimes for the path integral ground state Monte Carlo.

The trial wavefunction ψ is defined through a set of *variational parameters* $\{\alpha_i\}$ and the minimization implied by Eq. (1) is performed with respect to these parameters. Using a real space representation of the many-body wavefunction ψ ,

$$\langle \psi_{\{\alpha\}} | \hat{A} | \psi_{\{\alpha\}} \rangle = \int d\mathbf{r}_1 \cdots d\mathbf{r}_N \psi_{\{\alpha\}}^*(\mathbf{r}_1, \dots, \mathbf{r}_N) \hat{A} \psi_{\{\alpha\}}(\mathbf{r}_1, \dots, \mathbf{r}_N), \quad (3)$$

where \mathbf{r}_1 through \mathbf{r}_N denote coordinates of all particles in the system. In variational Monte Carlo, the multidimensional integral (3) is evaluated via a Monte Carlo integration scheme, and this constitutes the numerical challenge of the method.

The Monte Carlo integration of Eq. (3) is carried out by sampling of the configuration space¹

$$\mathbf{X} = \{\mathbf{r}_1, \dots, \mathbf{r}_N\}$$

with probability proportional to the non-negative density $\psi^*(\mathbf{X})\psi(\mathbf{X})$. Normalization implies that the distribution of samples in the configuration space is

$$P(\mathbf{X}) d\mathbf{X} = \frac{\psi^*(\mathbf{X})\psi(\mathbf{X})}{\langle \psi | \psi \rangle} d\mathbf{X}. \quad (4)$$

Averaging over this distribution the *local value* of an operator, defined as

$$A_L(\mathbf{X}) = \frac{\hat{A}\psi(\mathbf{X})}{\psi(\mathbf{X})},$$

yields the integral of Eq. (3) and thus the operator's expectation value (2).

In this work, the distribution of Eq. (4) is created with the Metropolis scheme [7]. The position in the configuration space \mathbf{X} is transformed to a position $\mathbf{X}' = D(\mathbf{X})$ and the new position is accepted with probability equal to the ratio of the probability densities in the transformed and original

¹Additional degrees of freedom are readily accomodated.

configurations. Thus the updated configuration is taken as

$$\mathbf{X}^{\text{updated}} := \begin{cases} \mathbf{X}', & \text{if } \frac{|\psi(\mathbf{X}')|^2}{|\psi(\mathbf{X})|^2} > \xi \\ \mathbf{X}, & \text{otherwise} \end{cases}, \quad (5)$$

where ξ is a pseudorandom number uniformly distributed on $[0, 1]$. The Markov chain produced with the acceptance criterion (5) provides configurations distributed according to the desired probability density (4).

We aim to describe the bulk properties of liquid helium-4. With a very good accuracy, helium atoms may be considered particle-like with a known pairwise interaction. The Hamiltonian is given by

$$\hat{H} = -\frac{\hbar^2}{2m_{He}} \sum_i^N \nabla_i^2 + \sum_{i<j}^N V(r_{ij}),$$

where m_{He} is the mass of the ${}^4\text{He}$ atom, N is the number of atoms in the system, and r_{ij} is the distance between particles i and j .

The form of the wavefunction which we implemented is a widely used Bijl-Jastrow product of pair correlation functions [8],

$$\psi(\mathbf{X}) = \prod_{i<j}^N e^{u(r_{ij})} = e^{\sum_{i<j} u(r_{ij})}. \quad (6)$$

We have implemented the parallelization for single-particle updates, where only one atom is displaced at a time to form the new configuration. The transformed (trial) configuration \mathbf{X}' is given by

$$\mathbf{X}' = \{\mathbf{r}_1, \dots, \mathbf{r}_{s-1}, \mathbf{r}_s + \boldsymbol{\delta}, \mathbf{r}_{s+1}, \dots, \mathbf{r}_N\},$$

where s is a randomly selected particle index and $\boldsymbol{\delta}$ is randomly selected displacement. Single-particle updates result in autocorrelation times in the generated Markov chain that only scale as the first order in the number of particles, and are preferable for VMC calculations of quantum liquids with large number of atoms. For single-particle updates of a system given by (6),

the acceptance probability in a Metropolis step (5) becomes

$$\frac{|\psi(\mathbf{X}')|^2}{|\psi(\mathbf{X})|^2} = \exp \left[2 \sum_{i \neq s} u(|\mathbf{r}_s + \boldsymbol{\delta} - \mathbf{r}_i|) - u(|\mathbf{r}_s - \mathbf{r}_i|) \right]. \quad (7)$$

We use the symmetrized form

$$u(r) = \begin{cases} \frac{f(r) + f(L - r)}{2f(L/2)} & , r \leq L/2 \\ 1 & , r > L/2. \end{cases} \quad (8)$$

The symmetrization length L is usually chosen as the smallest box dimension. Symmetrization results in a continuous first derivative of $\psi(\mathbf{X})$, removing corrections to the kinetic energy and allows to use alternative estimators for the energy. The pair-correlation factor $f(r)$ is chosen in the Schiff-Verlet form [9]

$$f(r) = -\frac{1}{2} \left(\frac{b}{r} \right)^5. \quad (9)$$

This function prevents the overlap of atomic cores. The power in r^{-5} is dictated by the helium-helium interaction potential at short distances and is nearly optimal. The parameter b is the only variational parameter in this wavefunction.

Much more complicated forms of the trial wavefunctions exist for strongly correlated quantum liquids and solids [10–13]. Even for the Jastrow form of Eq. (6), the pair function $u(r)$ can be considerably more complex and computationally expensive. Triple-correlation forms are also common [13]. For fermionic problems, a Slater determinant is necessary. However, additional arithmetics increase the parallel fraction of the program and only improves the parallelization outcome. The simple choice of the wavefunction is made with purpose to demonstrate the strength of the parallelization scheme.

3. CUDA framework

GPUs produced by Nvidia Corporation host up to several thousands cores and may be programmed for scientific applications with a specially developed

platform termed CUDA² framework. The GPU code presented here is written in the C implementation of CUDA, while the supporting code is provided in Fortran.

Single computing cores of the GPU are grouped into units called streaming multiprocessors (SM or SMX on Kepler architecture). Each SM contains additionally several special function units, a large amount of register space and a high-level user-managed cache called *shared memory*. A GPU unit typically includes between one and six GB of an on-board high-speed operating memory accessible to all SMs. This memory is called *global*.

A routine commanded by a CPU to be executed on a GPU is called a *kernel*. A kernel is executed by a certain number of *thread blocks*. Each thread block is resident on a multiprocessor and the threads within a block are easily synchronized. Communication and synchronization between different thread blocks is, however, slow and in principle not guaranteed by the language standard. To compute quantities to desired precision, it is productive to generate several independent Markov chains, each thread block working on its own walker. Only for very large systems, it becomes advantageous to use all multiprocessors simultaneously to work on a single Markov chain. Such a cooperating approach, with synchronization written along the lines of Ref. [14], has been successfully tried out but is not included here. Using multiple walkers is also more compatible with other QMC methods.

By design, each SM is capable of maintaining a very large number of threads with an intact register space for each thread, and can rapidly switch between the threads. Quite unlike for CPU, the GPU masks memory latency and the latency of mathematical units by switching between threads in a thread block and executing the instructions for the threads that are ready to proceed. It is thus favorable to run a very large number of threads on each SM, much larger than the actual number of single cores. We take advantage of this by partitioning the calculation of interparticle distances to different threads, each thread only computing several distances. The number of threads in a threadblock does not have to equal the number of particles.

Successive chunks of 32 threads, called *warps*, simultaneously execute the same instruction sequence but with their own data. Conditional branching within warps is possible but results in serialization. Thus all threads in a given warp are automatically synchronized. The *warp synchronicity* is heav-

²CUDA stands for “Compute Unified Device Architecture”.

ily exploited in the QL program, especially when performing parallel reduction such as for the sum of Eq. (7). This leads to a noticeable improvement in the execution times. The functionality can be switched by a preprocessor directive, as warp synchronicity is not strictly a part of the CUDA standard. Warp synchronicity is exercised on the thread level and it can be used even when the number of particles is not a multiple of the warp size.

GPU kernels may write directly to the host memory via the front-side bus. This process does not require terminating the kernel, allowing for shared memory persistence. All the caches and SM shared memory content and even registers may be kept intact. The data transfer to the host memory is also asynchronous with respect to the kernel’s execution. The kernel proceeds to the next operation after posting the memory command, even though the memory transaction completes thousands of cycles later. We take advantage of this feature by keeping the walkers in the shared memory, and occasionally “writing out” a copy to the central RAM. The SM proceeds to the next calculation immediately, and does not need to reload the coordinates. This feature was essential for achieving the reported performance.

Once a kernel is launched, control returns to the CPU, without waiting for the GPU task to finish. This capability is exploited to run the GPU and CPU parts of the code simultaneously. These are referred here as the GPU-side and CPU-side. The GPU performs the heavy number crunching; the code on CPU at the same time processes generated configurations and prepares raw random numbers for the next chunk of calculations. So long as the execution times of the CPU-side are shorter than those of the GPU, the load of CPU computations is almost completely masked. This is further discussed in Section 4.

4. Load masking, optimal execution and the modified Amdahl law

Variational Monte Carlo calculations can be seen as consisting of two interleaved tasks: generating the Markov chains to produce new configurations and then applying various operators to these configurations to extract the physical properties. We refer to the former as the generation steps, and to the latter as the analysis steps. N single-particle updates (sometimes called *microupdates*) constitute a *macroupdate* and separate configurations \mathbf{X}_j and \mathbf{X}_{j+1} in our notation. The cost of one microupdate includes computing N interparticle distances for the sum of Eq. (7). Thus the cost of performing

one macroudate is $\mathcal{O}(N^2)$, the same as that of a typical analysis step, but possibly with quite a different coefficient. The consecutive configurations are correlated, and one needs to decide the optimal number of macroudates to be performed between the analysis steps. Optimal conditions result in the smallest statistical errors for the available computer time.

Given m_c is the autocorrelation “time” between successive configurations, and configurations are only analyzed every m macroudates (that is, one only performs analysis on configurations $\mathbf{X}_j, \mathbf{X}_{j+m}, \mathbf{X}_{j+2m}, \dots$), the true uncertainty in the mean of a computed quantity is

$$\sigma = \frac{\sigma_0}{\sqrt{n_{\text{samples}}}} \sqrt{1 + \frac{2m_c}{m}}, \quad (10)$$

where σ_0^2 is the variance of the distribution of this quantity and n_{samples} is the number of analysis instances [15]. For a fixed computer time, n_{samples} is inversely proportional to the time between analyses t_{step} .

Let t_A be the time necessary for analysis, and t_G the time necessary to generate one macroudate. If both the generation and analysis are performed on the same unit, $t_{\text{step}} = t_A + mt_G$ and the optimization of Eq. (10) gives

$$m = \sqrt{2m_c \frac{t_A}{t_G}} = \sqrt{2m_c \alpha}, \quad (11)$$

where we introduced $\alpha = t_A/t_G$. By order of magnitude, α is close to unity. Consider now the asynchronous generation, in which the GPU generates new macroudates, and the CPU performs analysis on previously prepared configurations at the same time. The asynchronous time per analysis instance is

$$t_{\text{step}} = \max(mt_G, t_A),$$

and optimization of Eq. (10) yields, unsurprisingly,

$$m = \frac{t_A}{t_G} = \alpha, \quad (12)$$

that is, both CPU and GPU are used at all times, $t_A = mt_G$.

The load masking leads to a modified version of the Amdahl law. Suppose that R_{CPU} is the code fraction that remains on the CPU³, and the serial and

parallizable parts that are moved to the GPU are S_{GPU} and P_{GPU} . Thus

$$R_{\text{CPU}} + S_{\text{GPU}} + P_{\text{GPU}} = 1.$$

There is an additional overhead associated with launching the parallel process; it is omitted here for clarity. If the parallel portion of the GPU code may be accelerated by M processors of the GPU, the resulting speed-up is

$$A(M) = \frac{1}{\max(R_{\text{CPU}}, S_{\text{GPU}} + M^{-1}P_{\text{GPU}})}. \quad (13)$$

In the case of a complete CPU-side masking, acceleration reduces to

$$A(M) = \frac{1}{S_{\text{GPU}} + M^{-1}P_{\text{GPU}}} = \frac{M}{MS_{\text{GPU}} + P_{\text{GPU}}}, \quad (14)$$

with the CPU fraction completely removed from the equation. Because the serial component of Markov chain generation is much smaller than the serial fraction of the entire program, we have $S_{\text{GPU}} \ll R_{\text{CPU}} \ll 1$. Having isolated the serial GPU fraction S_{GPU} , we may focus on minimizing it by improving the program. In the absence of time masking, the acceleration is limited by $S_{\text{GPU}} + R_{\text{CPU}} \approx R_{\text{CPU}}$, and the CPU-side execution quickly becomes the bottleneck.

Even when the GPU performs both the generation and analysis, load masking improves the performance. For example, random numbers may be prepared by the CPU for the next block while the GPU is busy, as described below. Memory transactions through the system bus are also at least partially masked. An important consequence is that other, less computationally intensive tasks and analysis may remain on the CPU.

Optimal execution of the GPU code requires a careful selection of the number of walkers (and thus thread blocks), and the number of threads in each thread block. The number of walkers should be the maximum possible such that all thread blocks still remain simultaneously resident on the GPU. For smaller systems, number of threads equal to the number of particles is

³CPU side of the program need not be serial. It may, for example, use OpenMP acceleration to utilize all available CPU cores. In this case R_{CPU} corresponds to the combined time of the CPU execution, $R_{\text{CPU}} = S_{\text{CPU}} + D^{-1}P_{\text{CPU}}$, where D is the number of CPU cores.

optimal. However, reducing the number of threads has the benefit of smaller loop overheads (each thread serves several interparticle distances), reduced required register space and smaller temporary arrays (allowing for a larger number of resident thread blocks), and smaller cost of parallel reduction schemes. For this reason, large systems are best computed with the number of threads which is several times smaller than the number of particles. To make use of warp synchronicity, it is beneficial to use the number of threads such that it is a multiple of the warp size, equal to 32. The extra threads will be idle, but because of the GPU warp structure, such extra threads would be executed implicitly anyways. Finally, to save time on copying the random numbers to the GPU, it is best to use the largest number of steps which is allowed by the size of the GPU global memory.

5. Random numbers

A good uncorrelated sequence of numbers, also called pseudorandom, is crucial for a Monte Carlo integration. It was decided to separate the random number generation from the Markov chain generator. An entire sequence of “raw” pseudorandom numbers (uniformly distributed on $[0, 1]$) that is necessary for a large computational *block* is generated and placed in the GPU global memory. Such approach provides three advantages: 1). Pseudorandom (and truly random) number generators may be readily switched, making it easy to test new generators, especially those that work from the GPU. For the purpose of reliability, here we have used a standard generator on the CPU. 2). Generating a large quantity of random numbers at once is significantly faster than producing them one-by-one, because of a better pipeline utilization. 3). Numbers may be generated for the next block by the CPU while the CPU-side is waiting on the GPU kernel to finish. This is, in effect, a masking of CPU load with respect to the pseudorandom number generation, as described in Section 4.

It should be noted that the number of operations necessary to perform a macroupdate scales as $\mathcal{O}(N^2)$, while the number of necessary pseudorandom numbers is $5N$ (five numbers per microupdate: one number to pick the particle to be moved, three numbers for the displacement, and one number to make the update decision of Eq. (5)). Thus producing sufficient amount of random numbers is a challenge only for small systems. In practice, generating raw random numbers became a bottleneck only for systems with fewer than 256 particles. The program has a remarkable appetite for the random

numbers when computing small systems. For example, in the case of a 64-particle system with 128 walkers on a Tesla M2090 card, the GPU consumed over 100 million random numbers per second, rate limited by the generator. For such cases, one may opt for GPU-parallel generators, such as those provided by the CURAND library [16]. Such changes require minimal editing of the provided package.

The distributed package uses Fortran built-in generator which in principle depends on the compiler. We have used the code with the GNU Fortran compiler, which implements Marsaglia’s well-known KISS generator. The results were tested against the AMU sequence of true random numbers produced from vacuum fluctuation measurements [17]. The two sequences produced statistically identical results.

6. Implementation

In this section we discuss in more detail the workflow of the program. As described above, the part of the code that executes on the CPU is referred to as the CPU-side, and the GPU-side refers to execution on the graphical card. “Global memory” is the term used for the global memory of the GPU, and “host memory” refers to the main RAM of the computer.

Upon starting of the program, input files are read, which provide starting walker coordinates, box dimension, random sequence seed and execution parameters. The CPU-side allocates page-locked arrays in host memory and the necessary arrays in global memory of the GPU. The former are used to pass walker coordinates to and from the GPU, and the latter are used to supply the GPU with random numbers.

As Monte Carlo results are statistical in nature, the execution is broken into blocks. Values averaged during a block are written to a file and values from successive blocks may later be averaged and analyzed for correlation and standard deviation values [18]. Walker coordinates are also written to a file at the end of each block. Thus every block-end provides a natural restore point.

An instance at which the GPU writes walker coordinates into page-locked host memory is here called a *writeout*. Writeout also includes values such as the acceptance ratio, computed potential and kinetic energies. Each writeout occurs into a unique separate space in the host memory. In the beginning of a block, the program writes computationally impossible values into the

writeout arrays. For example, negative values for particle coordinates. After starting the GPU kernel, the CPU-side loops over the memory space until the area to which a given generation of walkers is destined has been written to. Freshly arrived data is then taken for processing. The behavior is assisted by forbidding host caching of the writeout arrays through the `cudaHostAllocWriteCombined` flag to the `cudaHostAlloc` command. While it is not guaranteed that the writeout data will even begin to arrive before the kernel finishes, we have tested this behavior on a range of systems and always observed properly completed, uncorrupted asynchronous writeouts. Because each writeout occurs to its reserved part of memory, *in the worst-case scenario the data will be received after the kernel finishes, preserving program correctness*. There is a build-in check in the program which warns the users in case when the kernel in fact executes synchronously⁴.

The execution of a block is outlined in Fig. 1. The CPU-side copies random numbers to the GPU, launches a GPU kernel for the Box-Muller transform, and after that, the main computation kernel. Once launched, the kernel loads walker coordinates from page-locked host memory, and begins to produce the Metropolis updates. Each thread block serves one walker, that is, one Markov chain of configurations. For each microudate, the thread block loads the random particle index j , the “dice” variable ξ , and three displacement coordinates $\boldsymbol{\delta}_j$ from the GPU global memory.⁵ Each thread computes distances from the updated particle to one or several other particles, and computes $u(|\mathbf{r}_j - \mathbf{r}_i + \boldsymbol{\delta}_j|) - u(|\mathbf{r}_j - \mathbf{r}_i|)$ (see Eq. (7)). Periodic boundary conditions are applied to all distances. After this, a parallel reduction scheme is invoked and the sum from all threads in a thread block is accumulated in the zeroth element of the array `thread_sum`. This thread makes the update decision according Eq. (5),

$$d \leftarrow \left\{ \exp \left[2 \sum_{i \neq j} u(|\mathbf{r}_j - \mathbf{r}_i + \boldsymbol{\delta}_j|) - u(|\mathbf{r}_j - \mathbf{r}_i|) \right] > \xi \right\}$$

⁴Asynchronous execution is automatically disabled, for example, in case of certain debugging flags to the compiler. Synchronicity may also be forced with a preprocessor variable.

⁵Notice that the decision variable is effectively prefetched as it is called at the beginning of the microudate. The value arrives before it is needed at the end of the microudate. Such a small difference may account for several percent of performance.

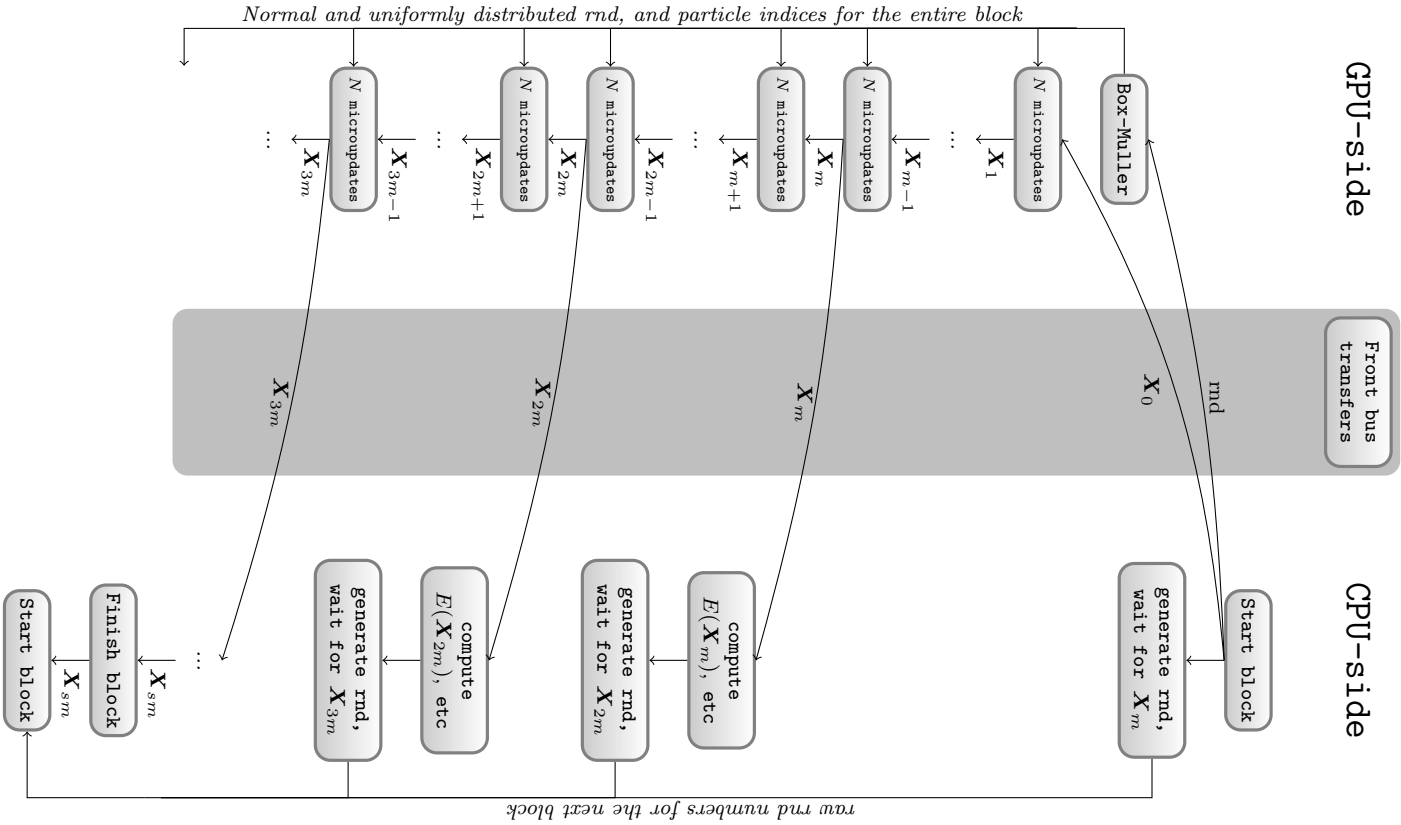


Figure 1: Block-diagram representation of the workflow. In this case, the CPU-side generates raw random numbers and sends them to the GPU-side for Box-Muller processing. Once the GPU obtains the starting walker configurations, it starts the Markov chain. Every m macroudates, the GPU sends the configurations back to the CPU for processing. Meanwhile, the GPU continues the generation. When the CPU-side is not occupied, it generates some raw random numbers to be used in the next block. A typical calculation consists of a considerable number of such blocks. Each block consists of an uninterrupted kernel, with configurations remaining in the shared memory. The size of a block is limited by the GPU global memory, typically at $2^{28} = 268 \cdot 10^6$ microupdates.

where the left-value is an integer variable and the logical right-value is evaluated as 1 when true and 0 otherwise. Update happens non-conditionally as

$$\mathbf{r}_j \leftarrow \mathbf{r}_j + \delta_j d$$

After the necessary number of updates, threads perform a writeout of walker coordinates and other necessary data. All threads participate in the memory command, with the data sequence ordered to ensue coalesced memory access.

Register-heavy routines for Kepler architecture

The Kepler K20 is the latest generation GPU from Nvidia. The Kepler chipset sports a considerably increased number of computing cores, but a reduced number of streaming multiprocessors (called SMX on Kepler). The amount of shared memory per multiprocessor is the same as in the previous, Fermi generation of GPU. Thus the amount of shared memory per card was reduced, while the number of cores has increased dramatically. Providing these cores with enough work proved to be a challenge. The issue was resolved by moving the walker data into the register space of the SMX. The Kepler chipset is equipped by 512 KB of register space per SMX, which is considerably larger than the available shared memory. Thus the walker data is broken into pieces, and each thread stores into its registers the coordinates for several particles of the walker. When a particle is moved in a trial move, the holding thread releases necessary coordinates to the rest of the threads through shared memory. This approach allowed to have considerably more resident walkers on an SMX, giving better occupancy of the GPU and increased performance. For benchmarking results, all K20 results were obtained with such *register heavy* routines. The routines are provided as part of the released program and may be selected through a preprocessor macro. In addition to improved performance, the use of the register space on the K20 allows to compute much larger systems, in excess of ten thousand atoms.

Quantum Liquids package

The CUDA routines that are described here are provided along with the Fortran code that is used to properly launch them. The resulting program is distributed as a package through the Computer Physics Communications Program Library. We refer to this program as the QL package. The QL package is a simplified version of a larger quantum fluids and solids package. The simplification allows us to focus on the GPU parallelization scheme.

However, only basic functionality in terms of observables is included. The supplied package files include a short manual. The manual lists the file structure of the program, input and output files, and control variables. Interested readers should refer to the manual for setting up the calculations.

The QL package is distributed in the form of a compressed `.tar` archive. Unpacking creates a directory called `ql`, which contains a makefile and the makefile configuration script, and a number of subdirectories. Compilation requires the CUDA compiler `nvcc` and the GNU Fortran compiler. Make should be invoked directly in the directory `ql`. For a standard Linux distribution, executing

```
make ql
```

in the command shell may be sufficient to compile the program. Alternatively, users may first run the configuration script, and execute

```
make configure
make clean
make ql
```

The configuration script tries to locate the libraries and necessary compilers.

Upon successful compilation, the user should be able to change to subdirectory `bin` and execute the program by entering

```
./ql
```

in the command prompt. The package is distributed with the input files that are ready to simulate liquid ${}^4\text{He}$ at its experimental equilibrium density, with 1000 particles and 16 walkers. The program should finish in less than three minutes. This sample run will execute 20 computational blocks, each block consisting of 100 analysis instances. Each analysis is separated by 4 macroupdates. Thus the sample run executes 128 million single-particle updates. During the execution, several data files are produced in the same directory. These include `e.dat` with the energy values from each block, `acceptance.dat` with the average Metropolis acceptance rates, and `final_config.dat` with the last walker coordinates. File `kinetic.dat` contains two independent estimates for the kinetic energy. The values in the second and third columns of this file should be statistically equal. File `store_seed.dat` contains the last used pseudorandom sequence seed. The details of the output file format are described in the provided manual, which

can be found in the subdirectory `ql/doc`. The contents of `e.dat` become as follows (not all digits are shown),

```

1      -5.8007   -20.9134    15.1127
2      -5.8122   -20.9253    15.1131
3      -5.7851   -20.9589    15.1738
...
19     -5.8102   -20.9566    15.1464
20     -5.7813   -20.9187    15.1373

```

The acceptance rates in file `acceptance.dat` become

```

1      0.3725
2      0.3727
3      0.3722
...
19     0.3720
20     0.3723

```

It should be noted that the produced output depends on the pseudorandom sequence used, and it is compiler-dependent. Only the averages of the computed values need to be equal to each other.

The parameters file `parameters.in` specifies the execution configuration, including the number of the computational blocks (field `blockstogo`), the number of analysis instances, or writeouts, in a block (`stepsinablock`), number of macroupdates between writeouts (variable m in Fig. 1; field `vmcmacrosteps`), dimensions of the simulation volume (field `bulkdimarray`), parameter b for the wavefunction (see Eq.(9); field `jastrowb`), particle mass in a.m.u. (`mass`), and the amplitude multiplier for the random displacements (`mtpstep`). Changes in these parameters do not require recompilation.

Variables that require recompilation are included in the form of preprocessor macros in the header file `setup.h`, which is located in the source directory `ql/src`. The number of particles, walkers, threads, and the functionality which is performed on the GPU are set in `setup.h`. The file `setup.pp` is the preprocessor header file that is used for the Fortran source files, and it is automatically produced by Make by stripping the comment lines from `setup.h`. Therefore, one should never have to edit `setup.pp`, which is automatically removed by Make after the compilation.

In order to accumulate sufficient statistics, it is often desirable to chain the execution of the Monte Carlo program. To do this, one has to copy the last walker coordinates and the last pseudorandom sequence seed into input files, by executing

```

cp final_config.dat configuration.in
cp store_seed.dat seed.in

```

After the copy commands, the program may be launched again and it will continue from the point at which it had last finished. Values for energy, acceptance rate, and pair distribution function histograms will be appended to the already existing data files.

7. Benchmarking conditions

The reported acceleration values are ratios of times measured for the GPU-parallelized and serial code executed on the same machine. We have decided to compare the execution of our CPU+GPU code to the execution on a single-core of a CPU, notwithstanding the fact that a GPU is usually accompanied by a powerful CPU with several cores. One may argue that the acceleration should be compared with a run which utilizes all available CPU cores. However, we find the single-core comparison appropriate for several important reasons. First of all, in practice, the calculations of the kind described here are so numerically demanding that they are performed on large clusters or supercomputers. The decision about using a GPU accelerator in such a case is guided by comparing available GPUs to an available allocation of core-hours on a supercomputer⁶. Second, the code that uses several cores needs to be parallelized, and questions may arise regarding the efficiency of such parallelization. Inefficient OpenMP implementations will artificially boost the apparent GPU acceleration numbers. A sceptical reader may always divide our results by the number of cores on the CPU, corresponding to an ideal OpenMP implementation, but the reverse is not possible without careful (and distracting) performance analysis of the CPU parallelization. Finally, single-core benchmarking is a widely accepted practice and allows for a better comparison with other works.

As the CUDA code was written, some routines were invariably optimized. For a fair comparison, the same routine was then written for the CPU. Thus the CPU-only program is optimized in good faith just like the GPU-CPU program.

The wavefunction that is used in this code is on purpose a rather simple one for its class. The mathematical load is small, while all the pair distances nonetheless need to be computed, and thus all the memory operations are

⁶For illustration, a 2-GPU system and $\times 70$ -times accelerated code is equivalent to a year-long allocation of 1.2 million CPU hours.

Table 1: Configuration of the computers used for benchmarking. The top column shows the labels used to refer to the corresponding machine in the text. M2090s were accessed on a BullX GPU cluster in the Barcelona Supercomputing Center. The 560Ti and K20 were installed on a workstation.

	560Ti	M2090	K20
Architecture	Workstation	BullX cluster	Workstation
CPU			
maker	Intel	Intel	Intel
type	i5-2500	Xeon E5649	i5-3570
clock frequency	3.3 GHz	2.5 GHz	3.4 GHz
memory	16 GB	24 GB	12 GB
L3 cache	6 MB	12 MB	6 MB
GPU			
series	GeForce	Tesla	Tesla
architecture	Fermi	Fermi	Kepler
chipset	GF114	T20A	GK110
model	GTX 560 Ti	M2090	K20
compute capability	2.1	2.0	3.5
number of cores	384	512	2496
SM(SMX) count	8	16	13
cores per SM	48	32	192
clock frequency	1.8 GHz	1.3 GHz	0.71 GHz
global memory	1.0 Gb	6.0 Gb	5.0 Gb

still necessary, along with the pseudorandom number generation. In practice, one often uses trial functions that are much more elaborated. Additional arithmetic complexity of the wavefunction in fact improves the parallel performance. In other words, we are testing the code with an unfavorable trial wavefunction.

Performance tests have been carried on several machines with different Nvidia GPU models. The computer specifications are summarized in Table 1. The GTX560Ti is a Fermi-architecture card from the GeForce family. It is a popular and very affordable card with excellent heat and noise control. Our 560Ti was overclocked by the manufacturer. The Tesla M2090 is a Fermi card designed specially for scientific computing. M2090s were accessed in the Barcelona Supercomputing Center, in a GPU cluster produced by Bull Inc. It should be noted that the Xeon processor accompanying the M2090 has a slower clock than the i5 CPUs in the other machines. This influences the acceleration ratios presented later, and one should be aware of this when trying to compare different cards. For this reason, absolute performance values are also shown. Finally, the Tesla K20 card was used in an Intel i5 workstation. The Tesla K20 is the latest Kepler architecture card from Nvidia. Kepler devices provide a significantly increased number of cores (in this case, 2496), a much larger register space, and instructions for improving global memory caching.

8. Results

Calculations were performed on a system representing liquid helium at its equilibrium density of 21.86 nm^3 . The wavefunction was of the Jastrow type (6), (8), (9), with the parameter b at optimum value $b = 0.307 \text{ nm}$. The single-particle displacement was Gaussian-distributed with a root mean square displacement of $0.5\rho^{-1/3}$, which results in the acceptance of roughly 40% of trial moves. The simulation box was always cubic with periodic boundary conditions, and the cutoff distance was set at half the box size. Calculations were performed on three different cards, as detailed in Section 7 and specified in Table 1.

8.1. Load masking

First we demonstrate masking of the CPU load by the GPU execution as described in Section 4. The calculations were made on the 560Ti card for eight independent Markov chains, one walker per SM. The GPU was used to

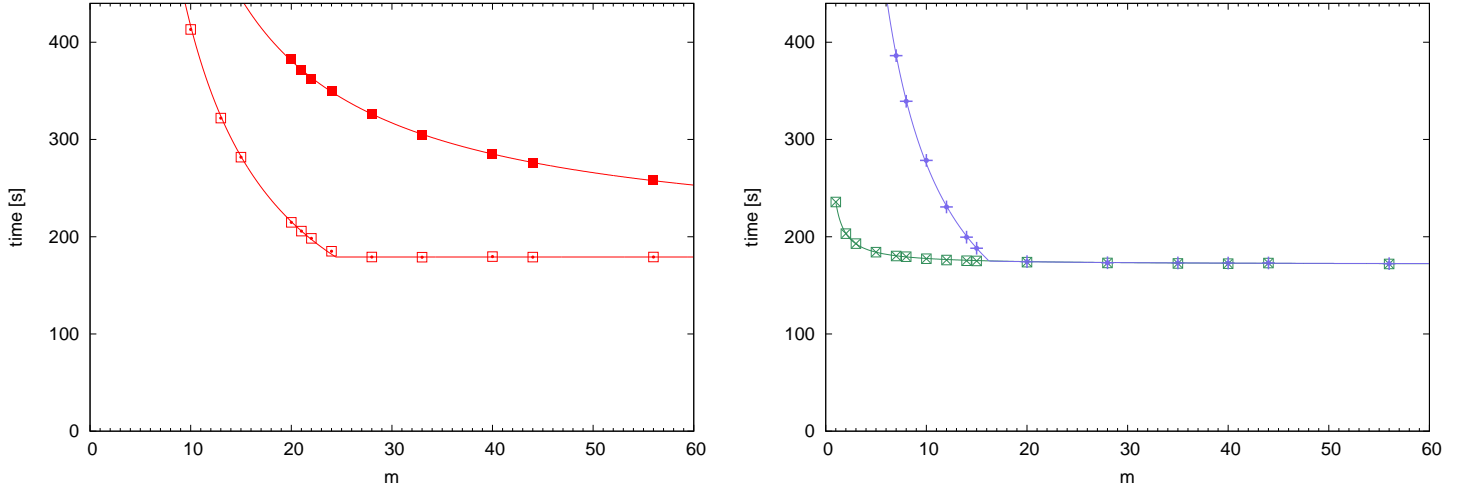


Figure 2: (Color online) Load masking for a calculation with 512 particles and eight independent Markov chains on a GTX560Ti. The total number of macroudates produced by the GPU for each chain was the same for each run and equal to 92400 (broken into 10 blocks). Every m macroudates, the configurations were written out to the host RAM and some analysis was performed. The vertical axis shows the total execution time in seconds. All lines are fits to the corresponding regions in the form $a+b/m$. *Left*: Configurations are produced by the GPU, energy is computed on the CPU. Filled squares show execution times for synchronous execution. Open squares are times for asynchronous execution with load masking as described in the text. *Right*: The GPU produces configurations and computes the energy. Green crossed boxes: CPU receives the configurations but does not perform any analysis. Blue crosses: The CPU receives the configurations and computes the pair distribution function. For $m > 20$, the calculation of the pair distribution function is completely masked.

execute the Box-Muller algorithm and then to generate new configurations, while the CPU-side generated the raw random numbers and performed energy calculations for configurations separated by a variable number of macroudates m . The total number of macroudates was kept fixed while the total number of analysis instances was varied. Thus the work performed by the GPU is not varied, and the needed number of random numbers is also fixed. Given the total number of macroudates is s (in this case, 10 blocks of 9240 macroudates), the number of writeouts and energy analyses is $w = s/m$. Thus the CPU time should be of the form $a + b/m$, where the constant b includes the cost of computing the energy.

The results are shown in the left panel of Fig. 2 with open boxes. As can

be seen, for small m the execution time is indeed very sensitive to m . In this region, the CPU time dominates, as it is larger than the GPU time. However, for $m > 25$, the CPU time becomes “undetectable” as it decreases below the GPU load. For a system with large autocorrelation times, such masking would allow to keep all the analysis calculations without parrallelizing them for the GPU, with no performance consequences. Moreover, any additional overhead on the CPU is also masked, in accordance with the modified Amdahl law of Eqs. (13)–(14). Notice also that the GPU-dominated region in Fig. 2 is perfectly flat, yet the number of configuration writeouts from the GPU to central RAM is decreasing as m^{-1} . The GPU is able to continue its work before the memory transaction is complete, and the cost of configuration writeouts is masked to the level of being negligible.

The liquid helium system that we consider has short autocorrelation times regardless of the system size. For optimum performance, the energy calculations had to be moved to the GPU as well. The right panel of Fig. 2 shows the resulting execution times (with green boxes). Now the GPU time consists of a constant generation time and the time for computing the energy which scales as m^{-1} . The same figure shows masking of another operator (with blue crosses). In that case, configurations and the energies are computed on the GPU, while the CPU performs calculations of the pair distribution function, a quantity of interest for such systems. Again there is a *masking threshold* in m above which the additional calculation comes at no cost.

8.2. Generation speed

In this section we look at the speed in which the GPU can generate new configurations. This is especially important for properties with large correlation times. The GPU was only used to generate new configurations, for as many independent Markov chains as was found optimal. In practice this meant up to 208 walkers for the smallest $N = 64$ systems on Kepler K20 (16 walkers per SMX). The optimal number of resident walkers per SM depends on the model of the GPU. For example, for the largest used $N = 1952$, Fermi M2090 was optimally ran with two walkers per SM (32 walkers in all), while Kepler K20 could be efficiently loaded with up to five walkers per SMX (65 walkers per card). For CPU-only execution, one chain is optimal to make the best use of the L1 cache. The results are shown in Fig. 3 in the form of times necessary to perform a macroupdate and the acceleration ratio for each GPU model.

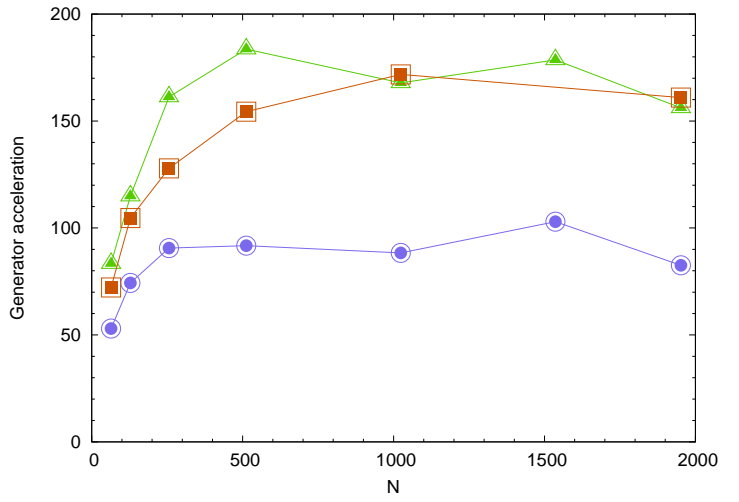
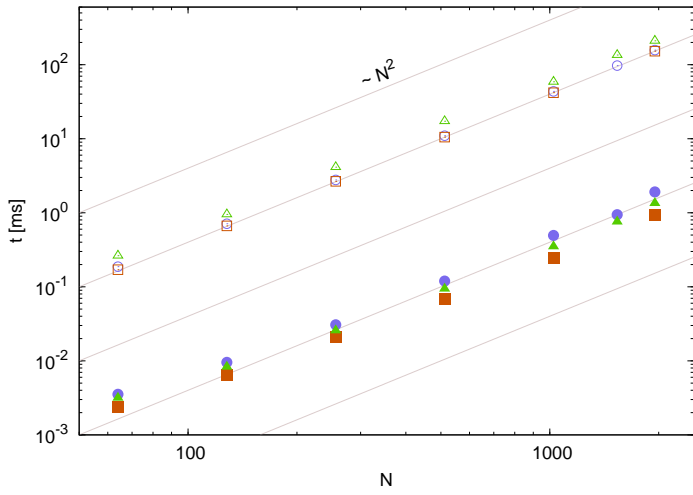


Figure 3: (Color online) Generation of new configurations by GPU compared to a single-core generation on CPU, for a varying number of particles N . The generation time is shown per macroudate per Markov chain. Blue bullets: 560Ti; green triangles: M2090; red squares: K20. GPU details are given in Table 1. *Left*: Absolute time, in milliseconds, necessary to perform a macroudate. Open symbols correspond to the CPU-only execution with a single core. Closed symbols: GPU-accelerated generation. Diagonal lines show $\sim N^2$ behavior. *Right*: Resulting acceleration ratios. Notice that generation times are in fact lowest for the K20 GPU

As can be seen, the acceleration is remarkable. Both for GPU and CPU, the macroudate generation time scales as N^2 , and the resulting acceleration is roughly constant and equal to $\times 85$ for the 560Ti card, and over $\times 150$ for M2090 and K20. However, performance is reduced for small systems, where random number generation becomes a limiting factor. The random number generation scales as $\mathcal{O}(N)$ and is masked for systems with more than 256 particles, as discussed in Section 4.

8.3. Full acceleration

Speed gains should ultimately be judged from the time that is necessary to compute the observables. We focus on the energy, while other properties have a similar computational complexity. To determine the acceleration, we compared execution times that are necessary to reach a given error level in the computed energy per particle. Both parallel and serial programs were ran with their respective optimal number of macroudates between analyses, determined empirically. Optimal execution is understood as such that leads to the smallest final uncertainty in the computed value of the observable, as described in Section 4. Because the GPU-accelerated and CPU-bound codes have different ratios of analysis-to-generation costs α , their optimal number of macroudates between analysis m are different (see Eqs.(11–12)). Benchmarking conditions are detailed in Section 7. Only one core was used on the CPU-side. For the accelerated code, the raw random numbers were generated on the CPU-side, while the GPU performed the Box-Muller transformation, generated new configurations and computed the energy values. The number of walkers was selected to provide the best occupancy for each particle count. The optimal number of walkers varies between the cards. Best results for K20 were achieved with 8 to 12 walkers per multiprocessor (between 104 and 156 walkers in total), even for the largest systems.

The acceleration results are shown in Fig. 4. The left panel shows the time, in seconds, that is necessary to reach the errorbar of 1 mK. In agreement with the central limit theorem, the product of the execution time t^{exec} and the square of the resulting error σ is an invariant,

$$t^{\text{exec}} \sigma^2 = \text{const.}$$

Both for the CPU-only and GPU-accelerated execution this constant scales with the first order of the number of particles N , due to self-averaging. This relation can be used to estimate the necessary execution time for a desired

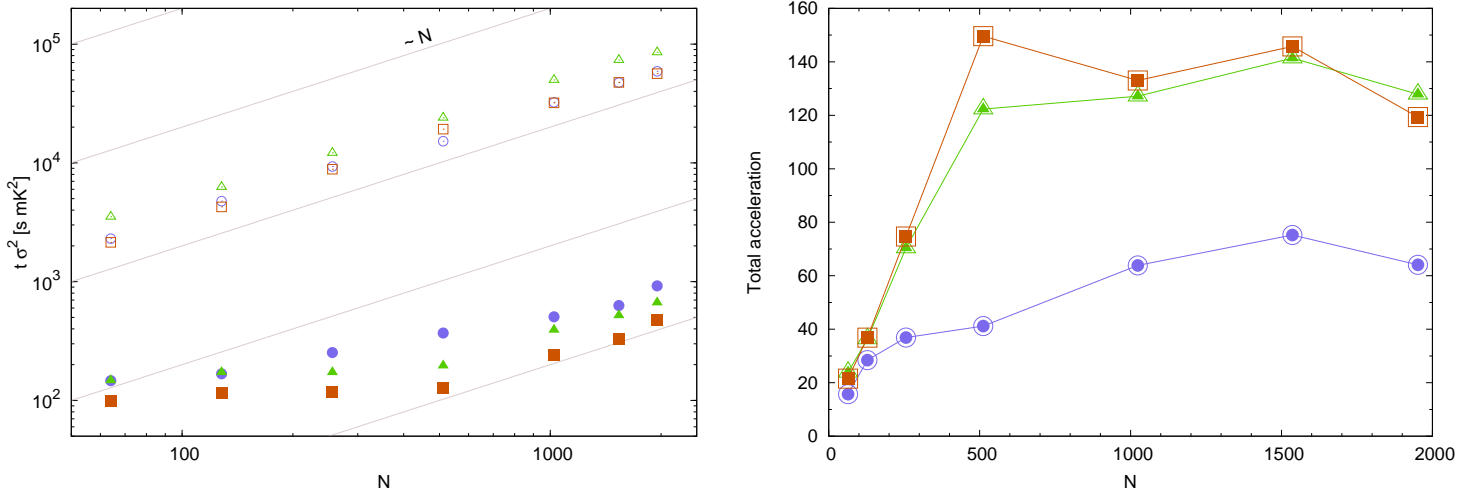


Figure 4: (Color online) The speed of computing the energy to a given accuracy. Blue bullets: 560Ti; green triangles: M2090; red squares: K20. *Left*: Time, in seconds, necessary to compute the energy with the error of 1mK per atom. Open symbols correspond to a single-core CPU execution, and closed symbols show GPU-accelerated execution. Lines show $\sim N$ behavior. *Right*: Resulting acceleration ratios for each card.

accuracy levels. At low particle numbers, acceleration is limited by the random numbers generation. As should be expected, this limitation is more severe for the higher-performance Kepler GPUs. For all GPUs, we observe linear scaling of the time-to-error for systems with more than 512 particles. For a 512-atom system, a 1 mK errorbar is reached in just over two minutes on Kepler K20 ($t\sigma^2 = 130 \text{ s} \cdot \text{mK}^2$), and in under four minutes on M2090 ($t\sigma^2 = 200 \text{ s} \cdot \text{mK}^2$). It is worth pointing out that this corresponds to a $2 \cdot 10^{-4}$ relative accuracy, more than satisfactory for most applications.

The right panel of Fig. 4 shows the resulting acceleration for each card. The values degrade for small particle number, as commented above. For systems with more than 500 atoms, acceleration ratios remain relatively constant. For the 560Ti, the value equals to $\times 50$, and for the Tesla M2090 and K20, acceleration exceeds a factor of $\times 120$. K20 was faster than M2090 for all system sizes.

8.4. Notes on the Kepler K20 performance

It is worth pointing out that the K20 was the best performing card. The execution times, shown in the left panels of Figs. 3 and 4, are smaller for the

K20 than for the other two cards. The acceleration, shown in the right panels of the two figures, seems larger for the M2090 because the individual CPU cores of the machine with the M2090 were slower, thus slightly inflating the acceleration. In fact, the K20 was as much as one-third faster than the M2090. This is remarkable given the already strong acceleration values for M2090. The improvement was achieved by using the register-heavy routines as described in Section 6. The extraordinarily large amount of register space on Kepler chips allowed to simultaneously process a larger number of walkers and thus keep the card occupancy high.

The second advantage of the large register space of the K20 is that it is capable of handling much larger systems when using the register-heavy routines, as described in Section 6. The scaling behaviors shown in Figs. 3 and 4 are preserved. For example, generating one macroudate for a 40960-particle calculation takes 418 ms (this number takes into account the fact that there were 13 walkers in total). The energy-computing kernel uses extra memory to store wavefunction derivatives; this kernel was used with up to 10240 particles. The ability to treat such large systems opens an access to a range of new applications for the method.

9. Conclusion

We have developed a remarkably efficient parallelization of bosonic variational Monte Carlo for graphical processing units. While VMC may be considered as the “junior” method among quantum Monte Carlo, it is mathematically lightest and thus hard to parallelize for GPUs. Up to two thousand particles may be treated with an Nvidia Fermi GPU, and up to ten thousands with Nvidia Kepler cards. Compared with a serial execution, acceleration over a factor of one hundred was consistently observed. Relative acceleration values in excess of one hundred should be considered with caution (consider using all CPU cores, or potential improvements to the serial code). However, the GPU produces excellent *absolute* speed results, which we measure as the time necessary to reach a level of statistical uncertainty in observables. The good acceleration values are mainly due to two developments. First and foremost, the execution was organized to allow for a shared memory persistence. The thread blocks of the GPU run uninterrupted for multiple steps, maintaining their walker information in shared memory or even in the register space. Second, the produced configurations are written out by the GPU to host memory for analysis as the calculation progresses.

The analysis on the CPU occurs simultaneously with the GPU generating the next configuration. This masks the CPU load and allows the developer to focus on improving the parallel fraction of the generating GPU kernel. The asynchronous execution results in a modified version of the Amdahl law. Existing CPU-based routines may be readily applied to the generated configurations, easing the transition to the GPU-parallel execution.

Acknowledgements

Author would like to thank the Barcelona Supercomputing Center (The Spanish National Supercomputing Center – Centro Nacional de Supercomputación) for provided GPU facilities.

References

- [1] S. Zhang, S. Yamagia, S. Yunoki, A study of parallelizing $O(N)$ Green-function-based Monte Carlo method for many fermions coupled with classical degrees of freedom, *J. Phys.: Conf. Ser.* 454 (1) (2013) 012049.
- [2] Y. Uejima, T. Terashima, R. Maezono, Acceleration of a QM/MM-QMC Simulation Using GPU, *J. Chem. Phys.* 32 (10) (2011) 2264.
- [3] R. K. Ragavan, GPU Acceleration of the Variational Monte Carlo Method for Many Body Physics, Master’s thesis, LSU (2013).
- [4] A. G. Anderson, W. A. Goddard III, P. Schroeder, Quantum Monte Carlo on graphical processing units, *Comp. Phys. Comm.* 177 (3) (2007) 298–306.
- [5] K. P. Esler, J. Kim, D. M. Ceperley, L. Shulenburger, Accelerating Quantum Monte Carlo simulations of real materials on GPU clusters, *Comput. Sci. Eng.* 14 (1) (2012) 40–51.
- [6] G. Amdahl, Validity of the single-processor approach to achieving large scale computing capabilities, in: *Proceedings of AFIPS Conference, 1967*, pp. 483–485.
- [7] N. Metropolis, S. Ulam, The Monte Carlo method, *J. Am. Statist. Assoc.* 44 (1949) 335–341.

- [8] R. Jastrow, Many-body problem with strong forces, *Phys. Rev.* 98 (5) (1955) 1479–1484.
- [9] D. Schiff, L. Verlet, Ground state of liquid Helium-4 and Helium-3 160 (1967) 208–218.
- [10] L. Reatto, Spatial correlations and elementary excitations in many-body systems, *Nuclear Physics A* 328 (1-2) (1979) 253.
- [11] P. Loubeyre, Three-body exchange interaction in dense helium, *Phys. Rev. Lett.* 58 (1987) 1857–1860.
- [12] Y. Lutsyshyn, C. Cazorla, G. E. Astrakharchik, J. Boronat, Properties of vacancy formation in hcp ^4He crystals at zero temperature and fixed pressure, *Phys. Rev. B* 82 (18) (2010) 180506.
- [13] K. Schmidt, M. H. Kalos, M. A. Lee, G. V. Chester, Variational Monte Carlo calculations of liquid ^4He with three-body correlations, *Phys. Rev. Lett.* 45 (1980) 573–576.
- [14] W.-C. Feng, S. Xiao, To GPU Synchronize or Not GPU Synchronize?, in: *IEEE International Symposium on Circuits and Systems (ISCAS)*, Paris, France, 2010.
- [15] D. P. Landau, K. Binder, *A guide to Monte Carlo simulations in statistical physics*, Cambridge University Press, UK, 2005.
- [16] CURAND library and documentaion is available from <https://developer.nvidia.com/curand>.
- [17] T. Symul, S. M. Assad, P. K. Lam, Real time demonstration of high bitrate quantum random number generation with coherent laser light, *Appl. Phys. Lett.* 98 (23).
- [18] H. Flyvbjerg, H. G. Petersen, Error-estimates on averages of correlated data, *J. Chem. Phys.* 91 (1) (1989) 461–466.